

Diffusion radius of muonic hydrogen atoms in H-D gas

Andrzej Adamczak*

Institute of Nuclear Physics, Polish Academy of Sciences, PL-31342 Kraków, Poland and

Rzeszów Technical University, PL-35959 Rzeszów, Poland

Jakub Gronowski†

Institute of Nuclear Physics, Polish Academy of Sciences, PL-31342 Kraków, Poland

(Dated: October 2, 2018)

Abstract

The diffusion radius of the $1S$ muonic hydrogen atoms in gaseous H_2 targets with various deuterium admixtures has been determined for temperatures $T = 30$ and 300 K. The Monte Carlo calculations have been performed using the partial differential cross sections for $p\mu$ and $d\mu$ atom scattering from the molecules H_2 , HD and D_2 . These cross sections include hyperfine transitions in the muonic atoms, the muon exchange between the nuclei p and d , and rotational-vibrational transitions in the target molecules. The Monte Carlo results have been used for preparing the time-projection chamber for the high-precision measurement of the nuclear μ^- capture in the ground-state $p\mu$ atom, which is now underway at the Paul Scherrer Institute.

PACS numbers: 34.50.-s, 36.10.Dr

*Electronic address: andrzej.adamczak@ifj.edu.pl

†Electronic address: jakub.gronowski@ifj.edu.pl

Theoretical studies of the muonic atom diffusion in molecular hydrogen-isotope targets are important for many experiments in low-energy muon physics. In particular, knowledge of the diffusion radius of muonic hydrogen atoms in gaseous H-D targets is required for investigations of the μ^- nuclear capture in the $p\mu$ and $d\mu$ atoms created in H-D targets. The diffusion radius R_{diff} is defined as the distance between the point of the muon stop in H-D and the point of the muonic atom disappearance due to the muon decay or to the muon nuclear capture. Since the μ^- capture rate on p or d is several orders of magnitude lower than the muon decay rate, R_{diff} is practically determined by the point of the muon decay. A high-precision measurement of the rate Λ_s for the muon capture $p\mu \rightarrow \nu_\mu + n$ in the ground-state $p\mu$ atom (MuCap experiment) is underway at the Paul Scherrer Institute [1, 2, 3, 4]. The rate Λ_s for the singlet state $F = 0$ of the total muonic atom spin F is sensitive to the weak form factors of the nucleon, especially to the induced pseudoscalar coupling constant g_P . As a result, this experiment will provide a rigorous test of theoretical predictions based on the Standard Model and low-energy effective theories of QCD [5, 6]. A high-precision measurement of the μ^- capture rate in the process $d\mu \rightarrow \nu_\mu + n + n$ is under consideration by the MuCap collaboration [3]. Such an experiment would be uniquely suited to study the axial meson exchange currents in the two-nucleon system.

In this paper, main results of the Monte Carlo simulations for determining the optimal conditions for the MuCap experiment are presented. The time-projection chamber is filled with almost pure H_2 gas which, however, contains a very small D_2 contamination. In the isotope exchange process $p\mu + d \rightarrow d\mu + p$, the energy of about 135 eV is released in the centre-of-mass system. Therefore, the created $d\mu$ atom gains the collision energy of a few tens eV. As a result, the diffusion radius is significantly enlarged. This leads to an enhanced absorption of the muons in the time-projection-chamber walls and limits the spatial resolution. The determination of the highest acceptable D_2 contamination has been one of the aims of the presented simulations. Since the capture rate Λ_s depends strongly on the total $p\mu$ spin, it is necessary to calculate the time evolution of the population of the $p\mu$ spin states. The initial distribution of the spin states $F = 1$ and $F = 0$ is statistical. The simulations have been performed for the target temperatures $T = 30$ and 300 K. The target density has been fixed at the constant value $\phi = 0.01$ (relative to the liquid hydrogen density of 4.25×10^{22} atoms/cm³), which corresponds to the pressure of about 9 bar at 300 K. At such a density, the probability of formation of the muonic molecule $pp\mu$ is small. In higher-density targets, the muon nuclear capture inside $pp\mu$ is significant. This leads to serious problems with interpreting the experimental data owing to inaccuracy of the rate for the ortho-para conversion of the $pp\mu$ molecules [1, 2, 3, 4, 5]. The spin-flip transition $p\mu(F = 1) + p \rightarrow p\mu(F = 0) + p$ due to the muon exchange between the protons is still sufficiently strong at $\phi \approx 0.01$ to ensure a fast quenching of the higher hyperfine state $F = 1$ and, therefore, an unambiguous Λ_s measurement.

The Monte Carlo kinetics code includes the muon decay, $p\mu$ and $d\mu$ scattering from the molecules H_2 , HD and D_2 , and formation of the molecules $pp\mu$, $pd\mu$ and $dd\mu$. In the scattering process, the atoms can change their spin states. The isotope exchange reaction $p\mu + d \rightarrow d\mu + p$ in $p\mu$ scattering from HD and D_2 is taken into account. Also, all possible rotational and vibrational transitions in the target molecules are included. At the collision energies $\varepsilon \lesssim 10$ eV (in the laboratory system), the scattering processes are described using the differential cross sections $d\sigma/d\Omega$ for scattering from the hydrogenic molecules [7, 8] (“molecular” cross sections). At higher energies, effects of the molecular binding and electron screening can be neglected and, therefore, the differential cross sections for the muonic atom

scattering from hydrogen-isotope nuclei are used [9, 10, 11, 12] (“nuclear” cross sections). In

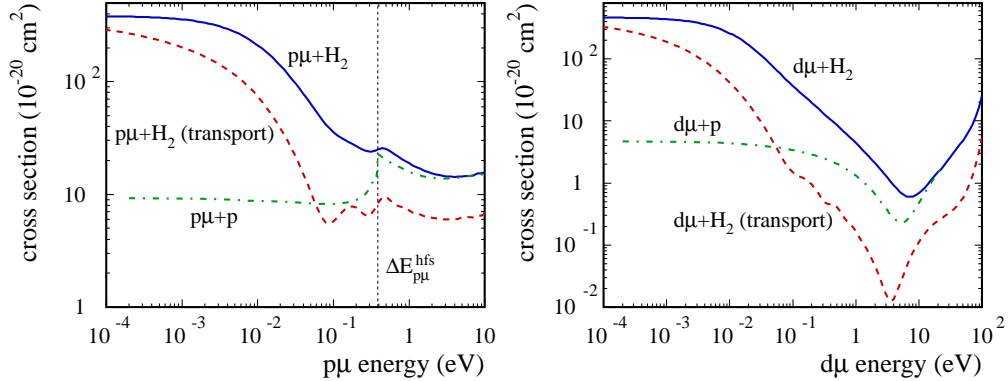


FIG. 1: Transport (dashed lines) and total (solid lines) cross sections for the scattering of $p\mu(F=0)$ and $d\mu$ atoms from a ground-state H_2 molecule versus the collision energy ε in the laboratory system. The doubled total cross sections (dash-dotted lines) for the corresponding nuclear scattering are shown for comparison. The hyperfine-transition threshold is denoted by $\Delta E_{p\mu}^{\text{hfs}}$.

fig. 1, the total molecular cross sections for $p\mu(F=0)$ and $d\mu$ scattering from the ground-state H_2 molecule are shown as an example. The muonic atom spin is conserved in the presented processes. Also, the corresponding transport cross sections, defined as

$$\sigma_{\text{tran}} = \int d\Omega (1 - \cos \vartheta) \frac{d\sigma(\vartheta)}{d\Omega}, \quad (1)$$

are shown. The scattering angle is denoted here by ϑ . The doubled total nuclear cross sections for the processes $p\mu(F=0) + p \rightarrow p\mu(F=0) + p$ and $d\mu + p \rightarrow d\mu + p$ are plotted for comparison. The transport cross sections approach the total cross section only at $\varepsilon \rightarrow 0$, which demonstrates strong anisotropy of the molecular cross sections. Large differences between the molecular and nuclear cross sections at $\varepsilon \lesssim 1$ eV are due to molecular-binding and electron-screening effects. The total molecular and nuclear cross sections for all combinations of the three hydrogen isotopes are presented in ref [13].

The time evolution of the hyperfine states, the energy distribution of the muonic atoms, and the radial distribution of the muon decays were calculated for various initial conditions. All the presented results are given for a fixed target density $\varphi = 0.01$. The initial distribution of the $p\mu$ or $d\mu$ kinetic energy was described by the two Maxwell components: thermal (50%) and energetic (50%) with the mean energy $\varepsilon_{\text{avg}} = 1\text{--}5$ eV, according to the experimental results [14, 15]. The calculated time evolution of the $F=0$ state and of the mean $p\mu(F=0)$ kinetic energy are shown in fig. 2, for a pure H_2 at $T = 300$ K. The $p\mu$ atoms starting at $\varepsilon \sim 1$ eV are slowed down within a few tens ns to energies where the spin-flip transitions $F=0 \rightarrow F=1$ are impossible. The hyperfine-transition threshold is $\Delta E_{p\mu}^{\text{hfs}} = 0.182$ eV in the $p\mu + p$ centre-of-mass system. After this time, the $F=1$ state disappears with a time constant of 6 ns. Hence, about 50 ns after the muon stop, the relative population of the $F=1$ state is below 0.01 and the measurement is no longer distorted by the population of the upper hyperfine level. All that takes place when most of the initially energetic atoms remains epithermal ($\varepsilon \gg k_B T$, where k_B is the Boltzmann constant). The $p\mu(F=0)$ thermalization from $\varepsilon \approx 0.1$ eV takes about 400 ns. As it is illustrated in fig. 3, the $p\mu(F=0)$ energy spectrum is epithermal for times much longer than in the case of $p\mu(F=1)$ atoms.

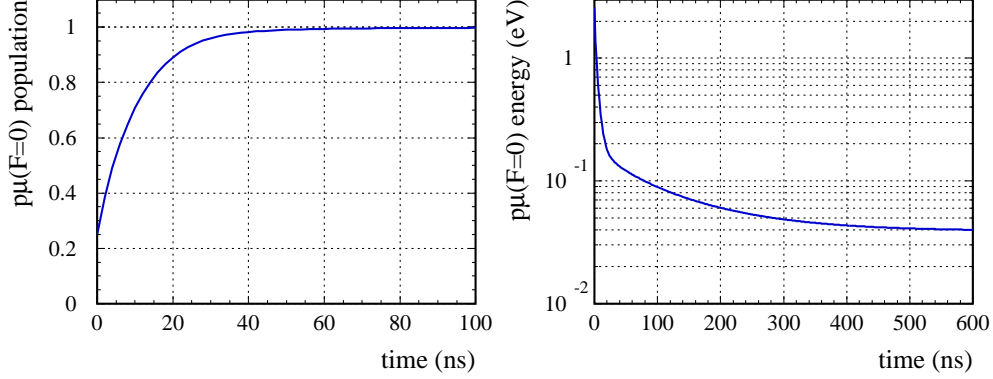


FIG. 2: Time dependence of the $p\mu(F=0)$ population and of the mean $p\mu(F=0)$ kinetic energy ε_{avg} in a pure H_2 at $T = 300\text{ K}$ and $\varphi = 0.01$.

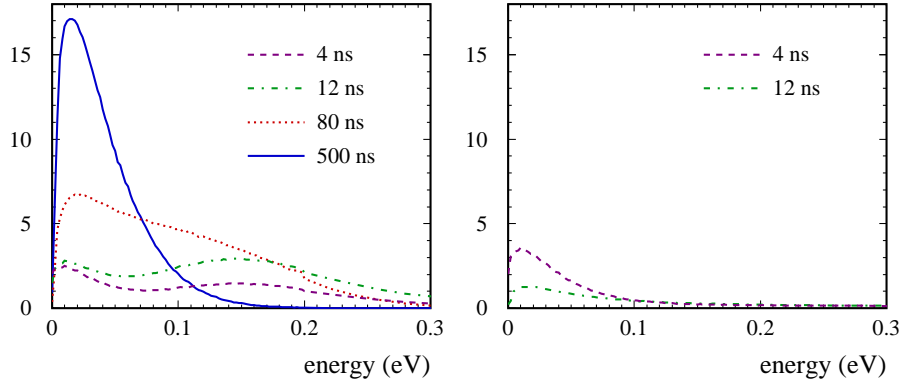


FIG. 3: Energy distribution of $p\mu(F=0)$ and $p\mu(F=1)$ atoms in a H_2 gas at $T = 300\text{ K}$, for several moments after the muon stop.

Only after the total deexcitation of the $F=1$ level, the $p\mu(F=0)$ energy distribution takes the final Maxwellian form with $\varepsilon_{\text{avg}} = 0.04\text{ eV}$. Most of the $p\mu$ diffusion until the muon decay takes place after the system has been thermalized.

The mean diffusion range, which is important for the optimisation of the pressure and temperature of H_2 filling the time-projection chamber, equals about 1 mm. However, long-lived ($t \gtrsim 10\ \mu\text{s}$) muons travel much farther, which limits the reachable spatial resolution. Figure 4 shows the fraction of the muon decays *outside* the diffusion radius from the point of $p\mu$ formation, for the target temperature of 30 and 300 K. The thermal diffusion is significantly reduced at 30 K. This effect is, however, limited because of the above-mentioned $p\mu$ acceleration in the spin-flip process. The radial distribution of the muon decays for several time intervals is plotted in fig. 5.

The calculated values of the mean diffusion radius for a pure H_2 target at $\phi = 0.01$ are summarised in table I. The results are given for $T = 30$ and 300 K. The realistic two-Maxwell distributions of the initial $p\mu$ energies have been used. Also, the thermalized initial distributions of $p\mu$ atoms with the depleted $F=1$ state have been employed in order to investigate the thermal part of the diffusion.

A real H_2 target always contains a certain admixture of deuterium. Figure 6 demonstrates that the maximal muonic atom diffusion radius is greatly increased when the deuterium

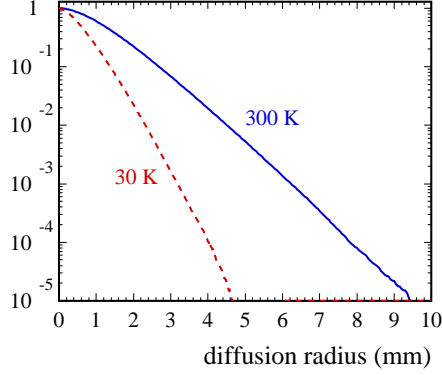


FIG. 4: Fraction of the μ^- decays *outside* the $p\mu$ diffusion radius from the point of $p\mu$ formation in a pure H_2 , for times $t \leq 20 \mu\text{s}$ and $T = 30$ and 300 K .

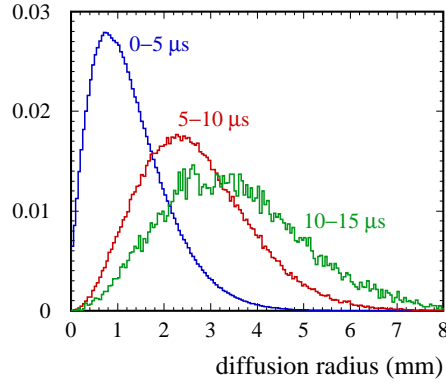


FIG. 5: Radial distribution of the μ^- decays for the time intervals 0–5, 5–10 and 10–15 μs at temperature $T = 300 \text{ K}$.

concentration of 10^{-4} – 10^{-3} is present in the H_2 target. The long-range tail in the radial distribution of the muon decays is due to very energetic ($\approx 45 \text{ eV}$) $d\mu$ atoms formed in the $p\mu$ collisions with deuterons. These $d\mu$ atoms can travel at large distances owing to the deep Ramsauer-Townsend minimum in the $d\mu + p$ cross section (see fig. 1). Therefore, it is crucial to reduce the deuterium concentration to a very low level of about 10^{-7} – 10^{-6} . The distribution of the $d\mu$ diffusion radius in a pure D_2 gas is shown in fig. 7 for $T = 30$

TABLE I: The calculated mean diffusion radius of the $p\mu$ atom in pure H_2 targets for various initial conditions and $\varphi = 0.01$.

Temperature	Initial ε distribution	mean R_{diff} [mm] for the time interval:			
		0–5 μs	5–10 μs	10–15 μs	15–20 μs
30 K	0.004 eV (50%) + 1 eV (50%)	0.68	0.88	0.99	1.11
300 K	0.040 eV (50%) + 5 eV (50%)	1.27	2.67	3.50	4.26
30 K	thermal, $F = 0$	0.23	0.51	0.68	0.82
300 K	thermal, $F = 0$	1.11	2.59	3.44	4.09

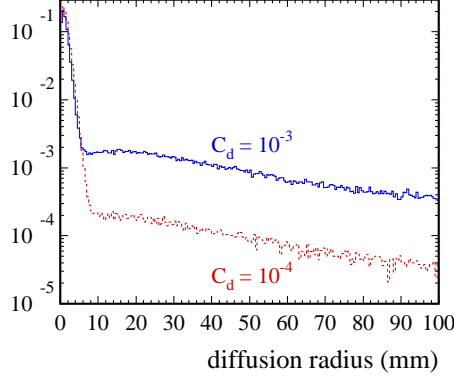


FIG. 6: Radial distribution of the μ^- decays in H_2 with the deuterium concentrations $C_d = 10^{-3}$ and 10^{-4} , for times $t \leq 20 \mu\text{s}$ and $T = 300 \text{ K}$.

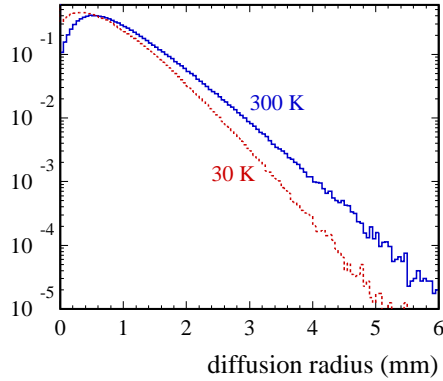


FIG. 7: Radial distribution of the μ^- decays from the point of $d\mu$ formation in a pure D_2 , for times $t \leq 20 \mu\text{s}$ and $T = 30$ and 300 K .

and 300 K and $\varphi = 0.01$. The mean value of R_{diff} is smaller (0.80 mm at 300 K and 0.65 mm at 30 K , for the time interval $0-5 \mu\text{s}$) than in the pure H_2 case since the elastic $d\mu(F = \frac{1}{2}) + d$ and $d\mu(F = \frac{3}{2}) + d$ cross sections are larger than the elastic $p\mu(F = 0) + p$ cross section [9]. Moreover, the hyperfine splitting for $d\mu$ is $\Delta E_{d\mu}^{\text{hfs}} = 0.0495 \text{ eV}$. As a result, there is practically no spin-flip acceleration of $d\mu$ atoms at 300 K . A relatively weaker acceleration, compared to the $p\mu + \text{H}_2$ case, takes place at 30 K .

The Monte Carlo results can be compared with a simple analytical estimation. The kinetic theory of gases gives the following mean diffusion radius $\overline{R}_{\text{diff}}$ as a function of time:

$$\overline{R}_{\text{diff}}^2 = 6Dt, \quad (2)$$

in which D denotes the diffusion coefficient. It is assumed that the atom survives until the time t . Using the standard definitions from the kinetic theory of gases:

$$D = \frac{vL}{3}, \quad L = \frac{1}{\sqrt{2}\sigma N}, \quad (3)$$

where v is the mean atom velocity, L is the mean free path, σ stands for the total cross section and N is the number density of atoms, one has

$$\overline{R}_{\text{diff}}^2 = \sqrt{2} \frac{vt}{\sigma N}. \quad (4)$$

The factor $\sqrt{2}$ is valid for a simple model of the hard sphere collisions. However, the muonic atom scattering from hydrogenic molecules is strongly anisotropic. Therefore, we use the following approximation:

$$\overline{R}_{\text{diff}} \approx \sqrt{\frac{vt}{\overline{\sigma}_{\text{tran}}N}}, \quad (5)$$

where $\overline{\sigma}_{\text{tran}}$ is the transport cross section (1) averaged over the thermal motion of the muonic atoms and of the target molecules. Taking into account the muon lifetime $\tau_0 = 2.2 \mu\text{s}$, we obtain the following estimation of the mean diffusion radius:

$$\overline{R}_{\text{diff}} \approx \sqrt{\frac{v\tau_0}{\overline{\sigma}_{\text{tran}}N}}. \quad (6)$$

For $T = 300 \text{ K}$, $\phi = 0.01$ and a pure H_2 target we have $\overline{\sigma}_{\text{tran}} = 20.8 \times 10^{-20} \text{ cm}^2$, which gives $\overline{R}_{\text{diff}} \approx 1.1 \text{ mm}$. The analogous estimation for $T = 30 \text{ K}$, using $\overline{\sigma}_{\text{tran}} = 161 \times 10^{-20} \text{ cm}^2$, leads to $\overline{R}_{\text{diff}} \approx 0.23 \text{ mm}$. These analytical values are in good agreement with the Monte Carlo results calculated assuming the thermal initial distribution of $p\mu$ energies and zero population of the $F = 1$ state (see the third column in table I). In the real case, the diffusion radius is larger owing to the epithermal diffusion. Let us note that it is very important to use the molecular differential cross sections for a correct Monte Carlo simulation of the thermal part of the diffusion. The diffusion radius in H_2 occurs to be about two times smaller than in the case when the corresponding nuclear cross sections are used.

In conclusion, it has been shown that the optimal conditions for studies of the μ^- capture on the proton inside the ground-state $p\mu(F = 0)$ atom are achieved at the target density $\phi \sim 0.01$ when the concentration of the deuterium is depleted to the level of 10^{-7} – 10^{-6} . The mean diffusion radius of the muonic atoms at these conditions is on the order of 1 mm. It can be significantly lowered when the target temperature is decreased from 300 K to 30 K. This effect is, however, limited as a fraction of the $p\mu(F = 0)$ atoms is epithermal both due to the initial high-energy component and to the deexcitation of the $F = 1$ states. The simulations of the muon capture experiments require using the differential cross sections for the muonic atom scattering from hydrogenic molecules. This is caused by strong molecular-binding and electron-screening effects at the collision energies below a few eV, where the main stage of the diffusion process takes place.

Acknowledgments

Drs. P. Kammel, V. E. Markushin and C. Petitjean are gratefully acknowledged for stimulating and helpful discussions.

-
- [1] P. Kammel *et al.*, Nucl. Phys. A **663-664**, 911c (2000).
 - [2] P. Kammel *et al.*, Hyperfine Interact. **138**, 435 (2001).
 - [3] P. Kammel *et al.*, *Proceedings of the International Conference on Exotic Atoms, EXA'2002*, Vienna, November 28–30, 2002, preprint nucl-ex/0304019.
 - [4] B. Lauss *et al.*, *Proceedings of the International Conference on Exotic Atoms, EXA'2005*, Vienna, February 21–25, 2005, preprint nucl-ex/0601004.

- [5] T. Gorringer and H. W. Fearing, *Rev. Mod. Phys.* **76**, 31 (2004).
- [6] J. Govaerts and J.-L. Lucio-Martinez, *Nucl. Phys. A* **678**, 110 (2000).
- [7] A. Adamczak, *Hyperfine Interact.* **82**, 91 (1993).
- [8] A. Adamczak, accepted for publication in *Phys. Rev. A*, preprint [physics/0608243](#).
- [9] L. Bracci *et al.*, *Muon Catalyzed Fusion* **4**, 247 (1989).
- [10] L. Bracci *et al.*, *Phys. Lett. A* **134**, 435 (1989).
- [11] L. Bracci *et al.*, *Phys. Lett. A* **149**, 463 (1990).
- [12] C. Chiccoli *et al.*, *Muon Catalyzed Fusion* **7**, 87 (1992).
- [13] A. Adamczak, *At. Data Nucl. Data Tables* **62**, 255 (1996).
- [14] D. J. Abbott *et al.*, *Phys. Rev. A* **55**, 214 (1997).
- [15] A. Werthmüller *et al.*, *Hyperfine Interact.* **103**, 147 (1996).